CONTENTS

Page

Acknowledgement d

Abstract in Thai e

Abstract in English h

List of Tables n

List of Figures p

List of Symbols u

Statement of Original in Thai w

Statement of Original in English x

Chapter 1 Introduction 1

1.1 Motivation 1

1.2 Basic Properties of Materials 4

1.2.1 Cu_2O 4

1.2.2 CuO 6

1.2.3 ZnO 8

1.2.4 Ethanol 10

1.3 Preparation of Copper Oxide Nanostructures by Various Techniques 11

1.4 Preparation of Copper oxide Nanostructures by Microwave 13

1.5 ZnO DSSCs 15

1.6 Research Objectives and Usefulness of the Research 16

1.6.1 Research Objectives 16

1.6.2 Usefulness of the Research 16

1.7 Thesis Organization 17

Chapter 2 Preparation and Characterization of Copper Oxide Nanostructures 18

2.1 Synthesis of Copper Oxide Nanofibers 19

2.2 Synthesis of Copper Oxide Nanoparticles 20

2.3 Characterization of Copper Oxide Nanostructures 21

2.3.1 Characterization of Copper Oxide Nanofibers 21

2.3.2 Characterization of Copper Oxide Nanoparticles 26

2.4 Chapter Summary 32

Chapter 3 Mechanisms of Copper Oxide Nanostructure Formation by Microwave-assisted Thermal Oxidation 33

3.1 Microwave Absorption 34

3.2 Plasma Phenomena 38

3.3 Nucleation 39

3.4 Structure Formation 41

3.5 Chapter Summary 46

Chapter 4 Copper Oxide Nanostructures in Dye-sensitized Solar Cells 47

4.1 Copper Oxide Nanofibers in ZnO DSSCs 47

4.1.1 Device Fabrication 47

4.1.2 Effects of Copper Oxide Nanofibers in DSSCs 48

4.2 Copper Oxide Nanoparticles in ZnO based DSSCs 57

4.2.1 Device Fabrication 57

4.2.2 Effects of Copper Oxide Nanoparticles in DSSCs 57

4.3 Comparison between Copper Oxide Nanofibers and Nanoparticles in ZnO based DSSCs 66

4.4 Chapter Summary 68

Chapter 5 Conclusions and Future Work 69

5.1 Conclusions 69

5.2 Comparison between this work and other works 72

5.3 Future Work 72

References 75

Appendix 89

Appendix A 91

Appendix B 99

Appendix C 103

Curriculum Vitae 106

LIST OF TABLES

		Page
Table 1.1	A brief overview of the basic physical properties of bulk Cu_2O.	6
Table 1.2	A brief overview of the basic physical properties of bulk CuO.	8
Table 1.3	A brief overview of the basic physical properties of bulk ZnO.	9
Table 1.4	A brief overview of the basic physical properties of ethanol.	11
Table 1.5	The advantages in copper oxide nanostructure preparation by different methods.	12
Table 1.6	Characteristics of copper oxide nanostructures preparation by microwave.	14
Table 2.1	Diameter ranges of copper oxide nanofibers at various heating times.	22
Table 4.1	Summary of ZnO DSSCs parameters including dye loading, short circuit current density (J_{SC}), open circuit voltage (V_{OC}) , fill factor (FF) and power conversion efficiency.	52
Table 4.2	Summary of electrochemical parameters of the ZnO DSSCs at different copper oxide concentrations including shunt resistance (R_{sh}), series resistance (R_s), charge transfer resistance (R_{ct}), and electron lifetime (τ).	55
Table 4.3	Summary of ZnO DSSCs parameters with CuO-Cu_2O nanoparticle layer.	60
Table 4.4	Summary of electrochemical parameters of the ZnO DSSCs at different copper oxide concentrations including shunt resistance (R_{sh}), series resistance (R_s), charge transfer resistance (R_{ct}), and electron lifetime (τ).	61

Table A.1 A comparison of the d_{hkl} from calculation with data base in program CaRIne v3.1. 98

Table C.1 Mechanisms of different polarizations. 103

LIST OF FIGURES

		Page
Figure 1.1	Number of DSSCs publications in recent years.	1
Figure 1.2	Cu_2O cubic structure.	5
Figure 1.3	CuO monoclinic structure.	7
Figure 1.4	ZnO structure of (a) hexagonal wurtzite and (b) cubic zincblend.	9
Figure 1.5	Structure formula of ethanol.	10
Figure 1.6	The principle operation scheme of the DSSC.	15
Figure 1.7	The principle operation scheme of the DSSC and recombination.	16
Figure 2.1	The flow chart of copper oxide nanostructures synthesized by microwave-assisted thermal oxidation.	18
Figure 2.2	(a) The effective mass yield of the copper oxide nanofibers prepared by a different masses of pure copper powders under microwave radiation, at 7 min and (b) copper oxide nanofibers in a quartz rod.	20
Figure 2.3	The percentage of copper oxide nanofibers obtained from reaction by using 1 g of copper powders at the different heating times.	20
Figure 2.4	SEM image of (a) CuO-Cu_2O nanofibers and (b) average lengths of CuO-Cu_2O nanofibers prepared from 1 g of copper powders under microwave radiation.	21
Figure 2.5	Size distribution of the CuO-Cu_2O nanofibers at the different heating times.	23
Figure 2.6	SEM image of CuO-Cu_2O nanofibers prepared at (a) 4 min, (b) 5 min (c) 6 min, (d) 7 min, (e) 9 min, and (f) 11 min under microwave radiation.	23

Figure 2.7 TEM images and electron diffraction patterns of CuO spot on a nanofiber. 24
Figure 2.8 Raman spectrum of the CuO-Cu_2O nanofibers synthesized at 4, 5, 6, 7, and 11 min under microwave radiation. 24
Figure 2.9 XRD patterns of the CuO-Cu_2O nanofibers prepared at 4, 5, 6, 7, and 11 under microwave radiation. 26
Figure 2.10 EDS spectrum of CuO-Cu_2O nanofibers at 7 min heating 26
Figure 2.11 The SEM images of the copper oxide nanostructures at 7 min by microwave heating using ethanol additive at (a) 0.0 mL (b) 0.2 mL (c) 0.3 mL and (d) 0.4 mL. 27
Figure 2.12 Size distribution of copper oxide nanostructures prepared against ethanol additive at (a) 0.0 mL (fibers), (b) 0.2 mL (nanoparticles), and (c) 0.3 mL (nanoparticles). 28
Figure 2.13 TEM images and electron diffraction patterns of (a) Cu_2O and (b) CuO nanoparticles. 29
Figure 2.14 Raman spectrum of copper oxide nanoparticles prepared against ethanol additive 0.2, 0.3, and 0.4 mL comparing to no ethanol (fibers). 30
Figure 2.15 XRD patterns of the copper oxide nanoparticles prepared against ethanol additive 0.0, 0.2, 0.3, and 0.4 mL under microwave heating. This results were plotted comparing to pure Cu, CuO, and Cu_2O powders. 31
Figure 3.1 Schematic of copper powders and copper powder-ethanol interactions under microwave radiation leading to morphological formation of mixed-phase copper oxide nanofibers and nanoparticles, respectively. 33
Figure 3.2 The flow chart of formation mechanism of copper oxide nanostructures synthesized by microwave-assisted thermal oxidation. 34
Figure 3.3 Schematic of (a) microwave-assisted synthesis of copper oxide nanostructures and (b) Cu particle-microwave

absorption showing volumetric penetration depth. 35
Figure 3.4 Schematic of (a) revolving and spinning electron of Cu atom and (b) induced electric field at Cu surface by a charge motion under microwave radiation. 37
Figure 3.5 Some parts of microwaves are absorbed by Cu and some parts are reflected leading to a localized overheating and power loss at the Cu surface. 38
Figure 3.6 Schematic of microwave – Cu particle interactions, (a) remarkably different voltages between the tips occurred, (b) electrons passing through the gap between the tips, and (c) plasma sputter around the Cu particles. 39
Figure 3.7 Total free energy as a function of nuclei size with degree of supersaturation. 41
Figure 3.8 The stable nuclei of copper oxide flowed up to the top surface of the quartz rod to form as a Cu_2O thin film 42
Figure 3.9 (a) Schematic and (b) real representation of Cu_2O/CuO nanofiber growth inside a quartz tube. 42
Figure 3.10 Electric dipole arrangements of ethanol (a) before and (b) after putting in electric field of microwaves. 43
Figure 4.1 Schematic diagram of ZnO DSSC structures with copper oxide nanofibers as a double layer in photoelectrode. 48
Figure 4.2 XRD patterns of copper oxide nanofibers comparing to Cu powders, CuO and Cu_2O powders. 49
Figure 4.3 SEM image of copper oxide nanofibers. 49
Figure 4.4 SEM images and EDS spectrum of ZnO nanopowders/ copper oxide nanofibers (3.42 mg/cm^2). 50
Figure 4.5 $J-V$ characteristics of ZnO DSSCs with different surface densities of copper oxide in photoelectrodes. 51
Figure 4.6 Power conversion efficiency (left) and current density (right) of ZnO DSSCs with copper oxide layer as a function of surface densities of copper oxide nanofibers layer in

photoelectrodes. 52

Figure 4.7 UV-vis absorption spectra of N179 dye-coated copper oxide nanofibers (3.42 mg/cm^2) on ZnO comparing to pure ZnO layer. 53

Figure 4.8 EIS spectra of ZnO DSSCs with different surface densities of copper oxide nanofibers layer. Experimental data are represented by solid symbols and solid lines correspond to fitted data. 54

Figure 4.9 (a) Schematic diagram of ZnO DSSC structures, (b) cross-section SEM images of ZnO/CuO-Cu_2O at 6 mM, (c) and (d) FE-SEM images of ZnO nanopowders and CuO-Cu_2O nanoparticles, and (e) schematic illustration of light scattering of ZnO/CuO-Cu_2O nanoparticles. 58

Figure 4.10 J -V characteristics of ZnO DSSCs with various concentrations of CuO-Cu_2O layer in photoelectrodes. 59

Figure 4.11 Power conversion efficiency of ZnO DSSCs with various concentrations of CuO-Cu_2O particle as additional layer in photoelectrodes. The efficiency of DSSC with pure CuO powders (6 mM) was compared. 59

Figure 4.12 Impedance spectra of ZnO DSSCs with different concentrations of CuO-Cu_2O layer and pure CuO layer at 6 mM, at forward bias voltage. 61

Figure 4.13 UV-vis absorption spectra of N179 dye coating on ZnO, ZnO/pure CuO (6 mM) and ZnO/CuO-Cu_2O (6 mM). 63

Figure 4.14 UV-vis diffused reflectance spectra of ZnO, ZnO/CuO (6 mM) and ZnO/CuO-Cu_2O (6 mM) (a) before and (b) after dye sensitization. 64

Figure 4.15 Impedance spectra of ZnO DSSCs with different concentrations of CuO-Cu_2O layer and pure CuO layer at 6 mM under dark condition with reward bias voltage. 65

Figure 4.16 Schematic image of V_{OC} in copper oxide nanostructures in

ZnO based DSSCs. 66

Figure 5.1 Flow chart of the main content in synthesis of mixed-phase copper oxide nanostructures and their application in ZnO DSSCs. 71

Figure A.1 (a) TEM image of a copper oxide nanoparticle and (b) the diffraction pattern of the nanoparticle with r. 92

Figure A.2 Data base of CuO to compare the d_{hkl}. 92

Figure A.3 Checked vectors for d_{hkl}. 93

Figure A.4 Cross vectors for $[uvw]$. 93

Figure A.5 (a) TEM image of a copper oxide nanoparticle and (b) the diffraction pattern of the nanoparticle with r. 95

Figure A.6 White spots sticking on the nanofibers and its diffraction patterns. 96

Figure A.7 Diffraction patterns of (a) the white spots in sample 1, (b) the white spots in sample 2, (c) the white spots in sample 3 and (d) the white spots in sample d. 97

Figure C.1 Loss tangent vector diagram. 104

LIST OF SYMBOLS

d	Skin depth
α	Attenuation factor
ω	Angular frequency of microwave
μ_0	Absolute permeability of free space ($4\pi\times10^{-7}$ H/m)
μ'	Magnetic permeability
ε_0	Absolute permittivity of free space (8.85×10^{-12} F/m)
ε''_{eff}	Effective relative dielectric loss factor
ε'	Relative dielectric constant
f	Microwave frequency
P_{EM}	Electromagnetic power absorbed per unit volume
E_{rms}	Root-mean-square values of electric field amplitudes
H_{rms}	Root-mean-square values of magnetic field amplitudes
T	Temperature in system
P	Power lost per unit area of surface
R_S	Surface resistivity
E_0	Electric field amplitude at the surface
η_0	Impedance of free space
r_c	Critical nucleus radius
r	Nucleus radius
ΔG	Total free energy of the system
ΔG_V	Free energy change per unit volume
γ	Free energy change per unit area of surface
k_B	Boltzmann constant (1.38×10^{-23} m^2 kg/ s K)
P_s	Equilibrium vapor pressure
P_V	pressure of supersaturated vapor
Ω	Atomic volume

S	Supersaturation
ΔG^*	Maximum energy barrier
H_S	Enthalpy of sublimation
N_A	Number of atom per one-mole crystal
N	Number of surface atom
A	Surface area
P_{tot}	Total of power lost per unit area of surface
$P_{dielectric\ loss}$	Loss power per surface area due to dielectric loss
δ	Phase lag
mM	Millimolar per litre

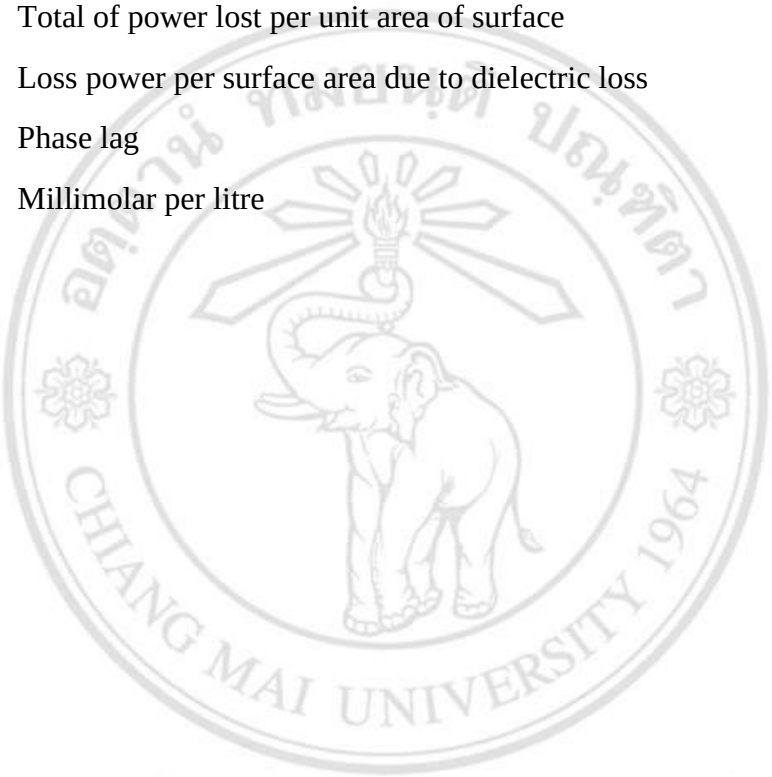

ข้อความแห่งการริเริ่ม

1. การสังเคราะห์เส้นใยนาโนคอปเปอร์ออกไซด์ ที่มีเฟสผสมของ CuO และ Cu_2O สามารถทำได้อย่างรวดเร็วโดยใช้ผงคอปเปอร์บริสุทธิ์เป็นสารตั้งต้น และใช้วิธีออกซิเดชันเชิงความร้อนที่ใช้ไมโครเวฟเป็นตัวช่วย

2. การสังเคราะห์อนุภาคนาโนคอปเปอร์ออกไซด์ ที่มีเฟสผสมของ CuO และ Cu_2O สามารถทำได้อย่างรวดเร็วโดยการเติมเอทานอลลงในผงคอปเปอร์บริสุทธิ์ และใช้วิธีออกซิเดชันเชิงความร้อนที่ใช้ไมโครเวฟเป็นตัวช่วย

3. เส้นใยนาโนคอปเปอร์ออกไซด์เกิดจากการสูญเสียความร้อนที่บริเวณผิวของอนุภาคคอปเปอร์ (conduction loss) เนื่องจากอันตรกิริยาระหว่างคลื่นไมโครเวฟและผงคอปเปอร์ ในขณะที่อนุภาคนาโนคอปเปอร์ออกไซด์เกิดจากการนำความร้อนที่บริเวณผิวของอนุภาคคอปเปอร์ (conduction loss) และการสูญเสียทางไฟฟ้า (dielectric loss) ของเอทานอล

4. การเคลือบโครงสร้างนาโนคอปเปอร์ออกไซด์ทั้งสองรูปแบบบนชั้นซิงก์ออกไซด์ของเซลล์แสงอาทิตย์ชนิดสีย้อมไวแสง ช่วยปรับปรุงประสิทธิภาพของเซลล์แสงอาทิตย์ให้ดีขึ้น

    4.1 สมบัติทางแสงของเฟสผสมของ CuO และ Cu_2O ในเส้นใยนาโนคอปเปอร์ออกไซด์ช่วยให้เซลล์แสงอาทิตย์มีช่วงการดูดกลืนแสงในช่วงอัลตราไวโอเลตที่กว้างขึ้น และพื้นผิวภายในขนาดใหญ่ของเส้นใยนาโนคอปเปอร์ออกไซด์ ช่วยเพิ่มการดูดกลืนสีย้อมไวแสงในเซลล์แสงอาทิตย์

    4.2 สมบัติทางแสงของเฟสผสมของ CuO และ Cu_2O ในอนุภาคนาโนคอปเปอร์ออกไซด์ช่วยให้เซลล์แสงอาทิตย์มีช่วงการดูดกลืนแสงที่กว้างขึ้น ด้วยอนุภาคที่มีขนาดใหญ่กว่า ZnO และด้วยความสม่ำเสมอของอนุภาคนาโนคอปเปอร์ออกไซด์ช่วยเพิ่มการเก็บเกี่ยวแสง (light-harvesting) ในเซลล์แสงอาทิตย์

STATEMENT OF ORIGINALITY

1. Copper oxide nanofibers consisting of mixed phases, CuO-Cu_2O, were simply and rapidly synthesized by using pure copper powders as a precursor via microwave-assisted thermal oxidation technique.

2. Copper oxide nanoparticles consisting of mixed phases, CuO-Cu_2O, were simply and rapidly synthesized by using ethanol addition in pure copper powders via microwave-assisted thermal oxidation technique.

3. Copper oxide nanofibers formed due to conduction loss by the microwave-Cu interaction at the Cu surface. Copper oxide nanoparticles formed due to the conduction loss and a dielectric loss of ethanol addition.

4. Coating both CuO-Cu_2O nanostructures, nanofibers and nanoparticles, on ZnO based DSSCs improve the DSSCs efficiency.

    4.1 The photovoltaic properties of the CuO-Cu_2O in the nanofibers can improve a wide absorbance in the visible light region. The large internal surface area of the nanofibers can improve more dye adsorption in the DSSCs.

    4.2 The photovoltaic properties of the CuO-Cu_2O in the nanoparticles can improve a wide absorbance in the visible light region. The larger homogenous size of the nanoparticle on smaller size of ZnO based layer in the DSSCs can improve light-harvesting in the DSSCs.